LASER INTERFEROMETER GRAVITATIONAL WAVE OBSERVATORY
- LIGO -
CALIFORNIA INSTITUTE OF TECHNOLOGY
MASSACHUSETTS INSTITUTE OF TECHNOLOGY

Technical Note	**LIGO-T1500325–v3**	2016/01/19

Frequency response of the aLIGO interferometer: part 1

Kiwamu Izumi and Daniel Sigg
for the aLIGO ISC group

Distribution of this document:

LIGO VIRGO scientific collaboration, and public

California Institute of Technology
LIGO Project, MS 100-36
Pasadena, CA 91125
Phone (626) 395-2129
Fax (626) 304-9834
E-mail: info@ligo.caltech.edu

Massachusetts Institute of Technology
LIGO Project, NW22-295
Cambridge, MA 02139
Phone (617) 253-4824
Fax (617) 253-7014
E-mail: info@ligo.mit.edu

LIGO Hanford Observatory
PO Box 159
Richland, WA 99352
Phone (509) 372-8106
Fax (509) 372-8137
E-mail: info@ligo.caltech.edu

LIGO Livingston Observatory
19100 LIGO Lane
Livingston, LA 70754
Phone (225) 686-3100
Fax (225) 686-7189
E-mail: info@ligo.caltech.edu

http://www.ligo.caltech.edu/

Contents

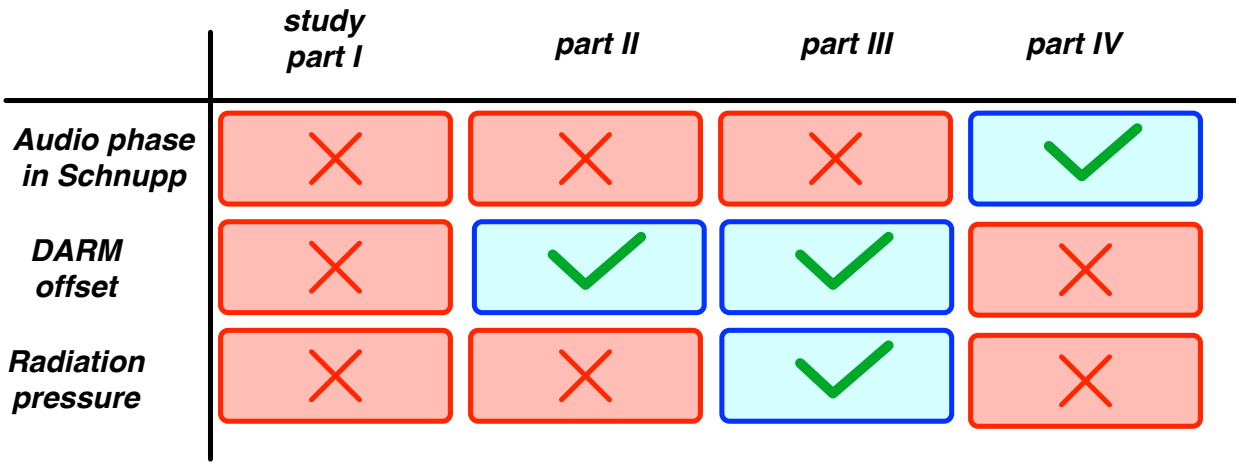

Figure 1: The (tetative) plan of the study. We plan to proceed with four steps. A red box indicates that the corresponding effect is not included while the blue boxes for the included.

1 Overview

1.1 Overview of the whole study

A goal of this study is to deliver clear and accurate picture of how we sense and control the length degrees of freedom (DOFs). For this purpose, we attempt to write down relevant interferometer responses as frequency responses in analytic form which should make underlying physics more apparent. We will intentionally start from a simple configuration and gradually add a few realistic complexities to our model as illustrated in figure 1. Throughout the study, we assume the electric fields to be plane-waves which propagate between well-aligned optics. Therefore neither mode-matching nor misalignment effects are considered.

1.2 Overview of this particular document

This document summarizes a first part of the study. As shown in figure 1, the results presented in this document are derived under the following assumptions that (1) audio sidebands in the Schnupp asymmetry do not rotate, (2) no DARM offset is introduced and (3) no radiation pressure effect is included. This configuration is equivalent to the previous study for iLIGO [1, 2]. Additionally, two arm cavities are assumed to be identical in this document. The effects from asymmetries between two arm cavities will be discussed in the next or later studies in a context of laser noises.

The outline of this document is as follows. In section 2, we explicitly define a number of relevant quantities for the later algebras. Section 3 gives a very brief introduction of how we derive the frequency response and states what approximations are enforced. In section 4, we discuss the frequency responses at the relevant signal ports. In section 5, we show that removal of the signal recycling mirror in the analytic expressions brings us back to the expressions for iLIGO without a conflict. Finally, we conclude this study in section 6 with some remarks for the next step. In addition, we compute the responses at DC independently of the main results for verification in appendix A.

2 Definitions and setup

2.1 Length degrees of freedom

We define the length DOFs as follows,

$$\begin{aligned}
\textbf{DARM: } L_- &= \frac{L_x - L_y}{2}, \\
\textbf{CARM: } L_+ &= \frac{L_x + L_y}{2}, \\
\textbf{PRCL: } l_\mathrm{p} &= l'_p + \frac{l_x + l_y}{2}, \\
\textbf{MICH: } l_- &= \frac{l_x - l_y}{2}, \\
\textbf{SRCL: } l_\mathrm{s} &= l'_s + \frac{l_x + l_y}{2}.
\end{aligned} \tag{1}$$

The optical distances are graphically shown in figure 2. Since we do not introduce a DARM offset or DC readout throughout in this document, the OMC is intentionally omitted in the figure. The frequency response of the DC readout is going to be discussed in the next and later parts of the study.

The macroscopic values of the lengths are summarized in table 3 in Appendix. To avoid confusions, here we explicitly note that the macroscopic value of the Michelson degree-of-freedom or Schnupp asymmetry is set to $l_\mathrm{sch} = (l_x - l_y)/2 = 0.04$ m. This definition is different from what we nominally use; the usual definition of Schnupp asymmetry is $l_x - l_y$ which gives 0.08 m [3].

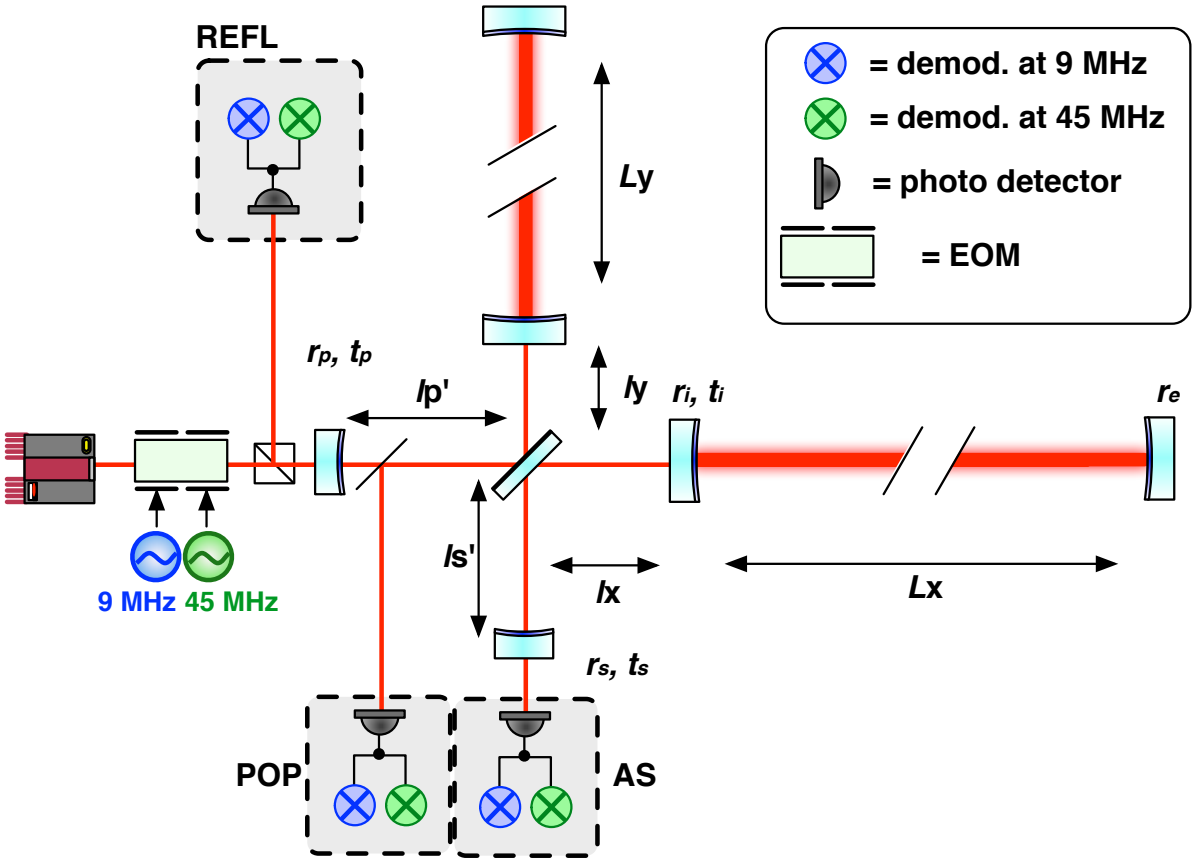

Figure 2: A schematic of the aLIGO interferometer setup.

2.2 Interferometric properties

We characterize the arm cavities by defining their reflectivities because we are always interested in the fields in reflection rather than that in transmission. We write the amplitude reflectivity as,

$$r_{\rm a} \equiv \frac{r_{\rm e}\,(t_{\rm i}^2 + r_{\rm i}^2) - r_{\rm i}}{1 - r_{\rm i} r_{\rm e}}, \quad \hat{r_{\rm a}} \equiv -\frac{r_{\rm e}\,(t_{\rm i}^2 + r_{\rm i}^2) + r_{\rm i}}{1 + r_{\rm i} r_{\rm e}}, \tag{2}$$

where the first one denotes the reflectivity for the carrier light which is resonant and the other for the rf sidebands which are assumed to be exact anti-resonant. Note that we use a sign convention such that the reflectivity for the carrier $r_{\rm a}$ is positive for an over-coupled cavity, as opposed to that of the previous study [1]. Additionally, the interferometric conditions for the carrier and rf sideband fields are summarized in table 1.

	arm cavities	**power recycling cavity**	**signal recycling cavity**
carrier	resonant	resonant	anti-resonant†
9 MHz rf sideband	anti-resonant	resonant	anti-resonant
45 MHz rf sideband	anti-resonant	resonant	resonant

Table 1: A summary of the interferometric conditions. We consider either exact resonance or exact anti-resonance for simplicity. † If ETMs are removed, the signal recycling cavity becomes resonant for the carrier light. This is also known as the resonant sideband extraction or RSE.

We also introduce derivative of the two reflectivities with respect to the round trip phase ϕ,

$$r'_{\rm a} = \frac{t_{\rm i}^2 r_{\rm e}}{(1 - r_{\rm i} r_{\rm e})^2}, \quad \hat{r_{\rm a}}' = \frac{t_{\rm i}^2 r_{\rm e}}{(1 + r_{\rm i} r_{\rm e})^2}, \tag{3}$$

where the first one represents that of the carrier and the other for the rf sidebands.

Apart from the arm cavities, we define reflectivity and transmissivity of the Michelson and signal-recycled Michelson interferometers for the rf sidebands as,

$$\begin{aligned} r_{\rm M}(\omega_{\rm m}) &= \hat{r_{\rm a}} \cos\left(2\frac{\omega_{\rm m} l_{\rm sch}}{c}\right), \quad t_{\rm M}(\omega_{\rm m}) = \hat{r_{\rm a}} \sin\left(2\frac{\omega_{\rm m} l_{\rm sch}}{c}\right), \\ r_{\rm sm} &= \frac{r_{\rm M} \mp \hat{r_{\rm a}}^2 r_{\rm s}}{1 \mp r_{\rm s} r_{\rm M}}, \quad t_{\rm sm} = \frac{t_{\rm s} t_{\rm M}}{1 \mp r_{\rm s} r_{\rm M}}, \end{aligned} \tag{4}$$

with $\omega_{\rm m}$ and $l_{\rm sch}$ being an rf modulation frequency and Schnupp asymmetry[1] respectively.

While $r_{\rm M}$ and $t_{\rm M}$ are valid for any modulation frequencies $\omega_{\rm m}$, the ones for the signal-recycled Michelson (i.e. $r_{\rm sm}$ and $t_{\rm sm}$) have two different expressions in order to represent the 9 and 45 MHz rf sidebands which have different resonant conditions in the signal recycling cavity as shown in table 1. The upper component of the $\pm$ and $\mp$ symbols in the equations represent that for the 9 MHz rf sideband while the lower components are for the 45 MHz rf sideband. For instance, $r_{\rm sm}$ for the 9 MHz sideband can be explicitly written as $\left(r_{\rm M} - \hat{r_{\rm a}}^2 r_{\rm s}\right) / (1 - r_{\rm s} r_{\rm M})$. This plus-and-minus convention is going to be used throughout the document.

[1] Again, we note that the definition of the Schnupp asymmetry in this document is given by $l_{\rm sch} = (l_x - l_y)/2$ following references [1, 2]. This definition is aligned to the definition of the canonical length degrees-of-freedom (1) which are all effectively in physical unit of single-trip length. There is another prevailing definition given as $l_x - l_y$ [4].

We define the reflectivity of the whole interferometer for both carrier and rf sideband fields as follows,

$$r_{\rm c} = \frac{\left(r_{\rm p}^2 + t_{\rm p}^2\right) r_{\rm a} - r_{\rm p}}{1 - r_{\rm p} r_{\rm a}}, \quad r_{\rm sb} = -\frac{\left(r_{\rm p}^2 + t_{\rm p}^2\right) r_{\rm sm} + r_{\rm p}}{1 + r_{\rm p} r_{\rm sm}}. \tag{5}$$

Note that the sign convention of the above two quantities is opposite from that in the previous study [1, 2]. Our convention here is such that when the carrier field is over-coupled, the reflectivity of the interferometer $r_{\rm c}$ is positive.

We finally define a few gains as follows,

$$g_{\rm p} = \frac{t_{\rm p}}{1 - r_{\rm p} r_{\rm a}}, \quad g_{\rm s} = \frac{t_{\rm s}}{1 + r_{\rm s} r_{\rm a}}, \quad g_{\rm sb} = \frac{t_{\rm p}}{1 + r_{\rm p} r_{\rm sm}}. \tag{6}$$

The first two gains are associated with the carrier – they are the power recycling and signal recycling gains respectively – and the last one is associated with the rf sidebands, representing the power recycling gain in the power recycling cavity.

2.3 Phase modulation

We apply phase modulations on the incident light with a cosine function rather than a sine. Therefore the incident field can be written as

$$E_{\rm inc} = E_0 \exp\left(i\omega_0 t + i\Gamma \cos\omega_{\rm m} t\right) = E_0 e^{i\omega_0 t}\left(J_0 + iJ_1 e^{i\omega_{\rm m} t} + iJ_1 e^{-i\omega_{\rm m} t}\right), \tag{7}$$

where ω_0, $\omega_{\rm m}$ and Γ are the carrier and rf modulation frequencies and a modulation depth respectively.

Even though we have two independent phase modulations (i.e. 9 and 45 MHz) which reduce the amplitude of all the frequency components due to inter-modulations, we ignore the inter-modulation effects and stick with equation (7) for simplicity. Therefore the amplitude of the carrier always stays at J_0 and the upper and lower rf sidebands stays at iJ_1 regardless of which rf frequency is considered.

3 Approach

3.1 Overview

We follow the method that M. Regehr summarized in his thesis [5] for deriving the frequency response. The purpose of this section is not only to briefly review the method, but also to give a sense of how to interpret the final results.

The method introduces a pair of audio sidebands which is excited by an oscillative displacement in a length DOF that we desire to know the response of. Subsequently we compute an amplitude transfer coefficient of the audio sidebands to a signal port which we desire to analyze. Converting the field at the photo detector into an observed intensity, one can obtain beatnote at around the rf modulation frequency ω_{m}. This is the signal we seek for.

In a coarse picture, the signals at the end of the calculation can be expressed in the form of

$$S = \left(\frac{\partial E^{(\mathrm{c})}}{\partial L_i} \otimes E^{(\mathrm{sb})} + E^{(\mathrm{c})} \otimes \frac{\partial E^{(\mathrm{sb})}}{\partial L_i} \right) \Delta L_i \left(\cos \omega_{\mathrm{m}} t + \sin \omega_{\mathrm{m}} t \right), \tag{8}$$

where $E^{(\mathrm{c})}$ and $E^{(\mathrm{sb})}$ represent complex amplitude of the carrier and rf sideband fields at the photo detector respectively. L_i is the excited length DOF. The $\otimes$ symbol is a (loosely defined) beat operator in order to give an idea of what combination of two fields are beating against. As written in the equation, the amplitude of the resultant signal is made of two beatnote components – one is made of a small change in the carrier field $\partial E^{(\mathrm{c})}$ beating against a static component of $E^{(\mathrm{sb})}$ and the other one made of the static carrier fied $E^{(\mathrm{c})}$ beating against a small change in the rf sideband $\partial E^{(\mathrm{sb})}$. In our frequency response analysis, a small change in the fields such as $\partial E^{(\mathrm{c})}/\partial L_i$ is dealt as a function of the excitation frequency ω. In other words, they are the audio sidebands that we excited by the oscillative displacement.

This coarse picture helps understanding behavior of the signals in the subsequent sections. For instance, as will be shown in section 4, the AS port does not have a static carrier field $E^{(\mathrm{c})}$ and therefore the resultant signal does not have contribution from the term $E^{(\mathrm{c})} \otimes \partial E^{(\mathrm{sb})}$.

3.2 Approximations for analytic expressions

When we derive analytic expressions for various frequency responses, we always make three major approximations as follows,

1. Neglect the time delays due to the propagation of the light.

2. Expand the expressions by $i\omega$ up to the first order.

3. Neglect phase rotation of the audio sideband for $l_{\rm p}$ and $l_{\rm s}$.

For instance, without these approximations, the response often comes in a form of

$$S \propto \frac{\text{const.}}{1 - re^{2i\omega L_1/c}} e^{-i\omega\Delta T} \tag{9}$$

where the denominator represents the interferometric amplification and the last exponential term represents a phase delay due to a propagation time of the light ΔT. Typically L_1 contains not only L_x and L_y, but also $l_{\rm p}$, $l_{\rm s}$. Assuming $l_{\rm p}$, $l_{\rm s} \ll L_x, L_y$, we drop $l_{\rm p}$ and $l_{\rm s}$ from the phase term. We also drop off the delay term and expand the amplification term up to the first order of $i\omega$ so that,

$$S \approx \frac{\text{const.}}{1 + i\omega/\omega_1}, \tag{10}$$

where ω_1 is defined as $c/\left(2L_1\right)|\ln\left(r\right)|$ in this instance.

As will be seen in the next section, we additionally perform numerical calculation for all the responses without these approximations. They provide us an idea of how accurate the analytic expressions are under the above approximations.

4 Frequency responses

Following the previous convention [2], we normalize all the responses by $S_0 = 2J_0J_1P_{\rm in}$.

4.1 AS port

The AS port sees only the differential modes (i.e. DARM and MICH) due to the perfect symmetry in the Michelson. Regardless of what modulation frequency we use, the signals are made only of a product of small change in the carrier field beating against the static rf sideband fields i.e. $dE^{(\rm c)} \otimes E^{(\rm sb)}$. This is because that we do not have a static carrier field at the AS port. Therefore the frequency response is completely determined by the behavior

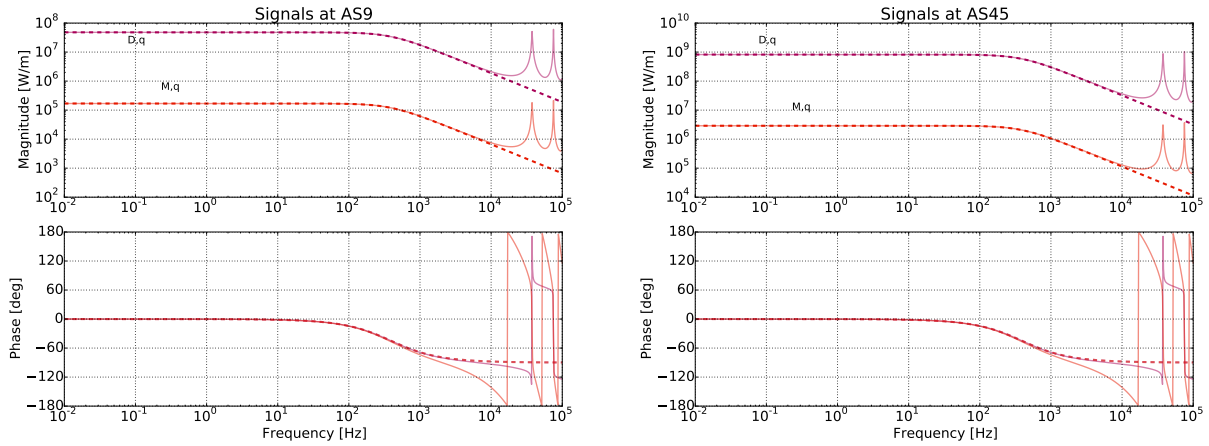

Figure 3: Frequency response at the AS port. The dashed lines indicate responses derived by the analytic expressions in equation 11. The solid lines are responses numerically computed without the approximations. The annotation letters indicate the following signals, *D,q*; DARM q-phase, *M,q*; MICH q-phase.

of the carrier light which brings the cavity pole into the equation while the amplitude of the signal scales with the transmissivity of the rf sidebands i.e. $g_{\rm sb}t_{\rm sm}$. The response can be summarized as

$$\begin{aligned}\frac{S^{(\rm as)}}{S_0} =& -4g_{\rm p}g_{\rm s}g_{\rm sb}r'_{\rm a}t_{\rm sm}\frac{1}{1+i\omega/\omega_{\rm rse}}k\Delta L_-\sin\omega_{\rm m}t \\ & -4g_{\rm p}g_{\rm s}g_{\rm sb}r_{\rm a}t_{\rm sm}\frac{1}{1+i\omega/\omega_{\rm rse}}k\Delta l_-\sin\omega_{\rm m}t.\end{aligned} \tag{11}$$

where $\omega_{\rm rse}$ is the sideband-resonant-extracted DARM cavity pole, defined as

$$\omega_{\rm rse} = \frac{c}{2L}\ln\left(\frac{1-r_{\rm i}r_{\rm s}}{r_{\rm e}r_{\rm i}-r_{\rm e}r_{\rm s}\left(t_{\rm i}^2+r_{\rm i}^2\right)}\right), \tag{12}$$

with L being the average length of the two arm cavities, defined as $L = \left(L_x + L_y\right)/2$. The MICH signal is also filtered by the same cavity pole because the filter effect comes when the field is reflected by the arm cavities.

As we will discuss in the next or later part of the study, the AS port will start seeing other DOFs as we will break the symmetry by introducing a DARM offset and etc.

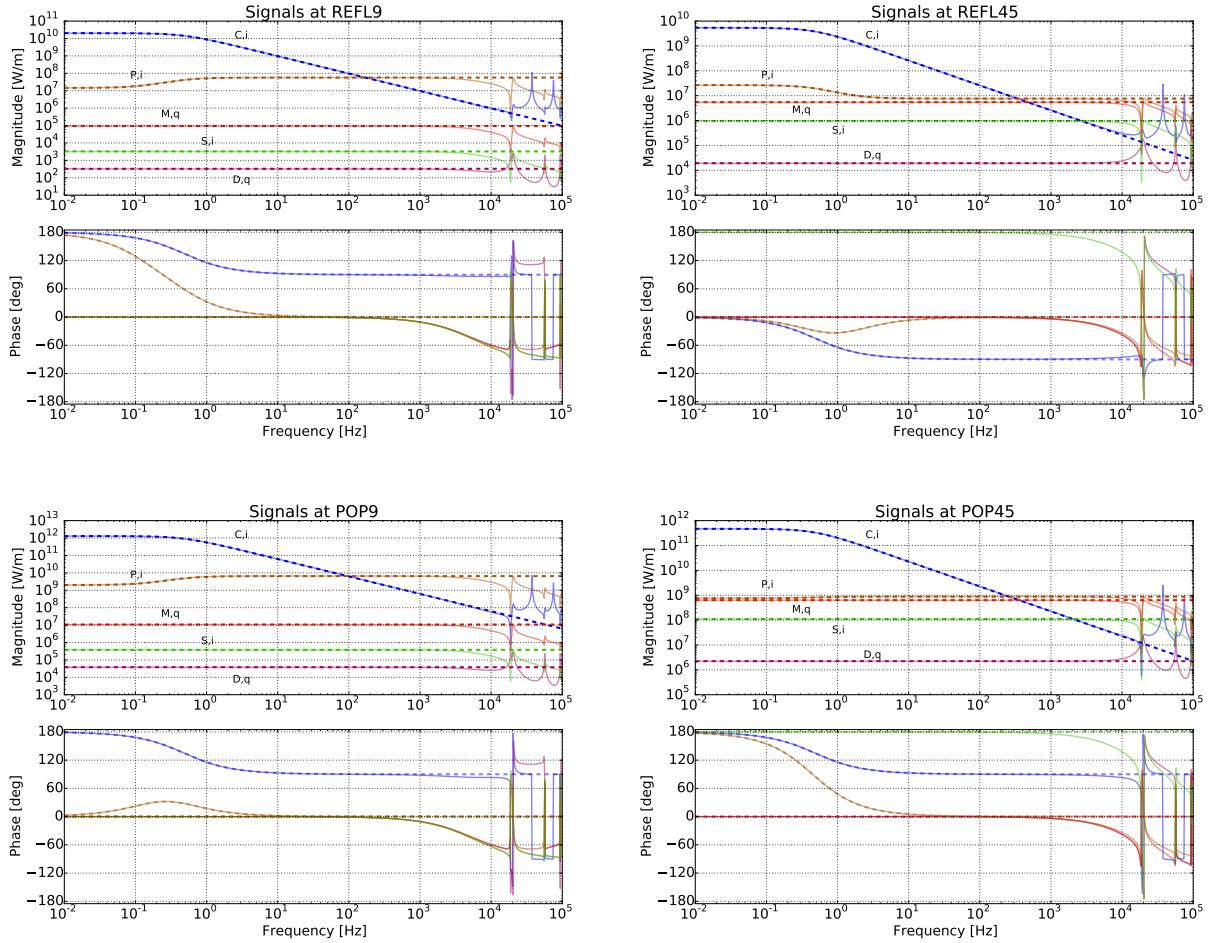

Figure 4: Frequency response at the REFL and POP ports. The dashed lines represent responses derived by the approximated analytic forms, and the solid lines are the ones numerically computed without the approximations. The annotation letters indicate the following signals, *C,i*; CARM in-phase, *D,q*; DARM q-phase, *M,q*; MICH q-phase, *P,i*; PRCL in-phase, *S,i*; SRCL in-phase.

4.2 REFL port

Unlike the AS port, the REFL port contains information of all five DOFs. The response can be written as

$$\begin{aligned}\frac{S^{(\mathrm{refl})}}{S_0} =& -4g_{\mathrm{p}}^2 r'_{\mathrm{a}} r_{\mathrm{sb}} \frac{1}{1+i\omega/\omega_{\mathrm{cc}}} k\Delta L_+ \cos\omega_{\mathrm{m}} t \\ &+ 4g_{\mathrm{sb}}^2 r_{\mathrm{c}} \hat{r_{\mathrm{a}}}' \chi k\Delta L_- \sin\omega_{\mathrm{m}} t \\ &- 4g_{\mathrm{sb}}^2 r_{\mathrm{c}} \hat{r_{\mathrm{a}}} \chi k\Delta l_- \sin\omega_{\mathrm{m}} t \\ &- 4\left(g_{\mathrm{p}}^2 r_{\mathrm{a}} r_{\mathrm{sb}} + g_{\mathrm{sb}}^2 r_{\mathrm{c}} r_{\mathrm{sm}}\right) \frac{1+i\omega/\omega_{\mathrm{r}}}{1+i\omega/\omega_{\mathrm{cc}}} k\Delta l_{\mathrm{p}} \cos\omega_{\mathrm{m}} t \\ &\pm 4\frac{g_{\mathrm{sb}}^2 r_{\mathrm{c}} r_{\mathrm{s}} t_{\mathrm{sm}}^2}{t_{\mathrm{s}}^2} k\Delta l_{\mathrm{s}} \cos\omega_{\mathrm{m}} t.\end{aligned} \tag{13}$$

where χ represents a coupling of the differential modes to the rf field on the reflection side, defined as

$$\chi \equiv \frac{1 - r_{\rm s}^2 \hat{r_{\rm a}}^2}{\left(1 \mp r_{\rm s} r_{\rm M}\right)^2} \sin\left(\frac{2\omega_{\rm m} l_{\rm sch}}{c}\right). \tag{14}$$

As for the $\mp$ symbol in the denominator, $-$ represents the 9 MHz and $+$ for the 45 MHz. This is a new quantity compared to iLIGO essentially because of the signal recycling. If we take out the signal recycling mirror, it reduces to a simple Michelson so that χ becomes $\sin\left(2\omega_{\rm m} l_{\rm sch}/c\right)$. The denominator tells us that an audio field excited by the differential modes experiences the amplification by the signal recycling cavity.

The CARM signal is the largest among the five as seen in figure 4 at low frequencies. The pole frequency is defined as

$$\omega_{\rm cc} = \frac{c}{2L} \ln\left(\frac{1 + r_{\rm i} r_{\rm p}}{r_{\rm e} r_{\rm i} + r_{\rm e} r_{\rm p}\left(r_{\rm i}^2 + t_{\rm i}^2\right)}\right). \tag{15}$$

This is typically as low as $\omega_{\rm cc}/\left(2\pi\right) \sim 1$ Hz in the case of aLIGO. As summarized in table 2, the CARM signal is made of mainly $dE^{\rm (c)} \otimes E^{\rm (sb)}$ and so for the reason the frequency dependency is mostly determined by how the carrier field behaves in the power-recycled common mode of the arm cavities.

The DARM and MICH responses show flat responses up to several kHz or so. This is because that they are made of $E^{\rm (c)} \otimes dE^{\rm (sb)}$. Since the rf sidebands are anti-resonant in the arm cavities, they essentially do not have a cavity pole effect. Even though the REFL port is rich for a static rf sideband, the audio sidebands of the carrier $dE^{\rm (c)}$ does not transmit to the REFL due to the perfect asymmetry in the Michelson and hence no $dE^{\rm (c)} \otimes E^{\rm (sb)}$ (also see table 2). The only difference between the DARM and MICH responses is a scaling factor – DARM is greater than MICH by a factor of $\hat{r_{\rm a}}'/\hat{r_{\rm a}}$.

The PRCL signal is complicated because it is made of not only $dE^{\rm (c)} \otimes E^{\rm (sb)}$, but also $E^{\rm (c)} \otimes dE^{\rm (sb)}$ as noted in table 2. Since the audio sidebands of the carrier have a double cavity pole while that of the rf sidebands do not, summing such two signals results in a pair of pole and zero. The zero can be written as

$$\omega_{\rm r} = \omega_{\rm cc}\left(1 + \frac{g_{\rm p}^2 r_{\rm a} r_{\rm sb}}{g_{\rm sb}^2 r_{\rm c} r_{\rm sm}}\right). \tag{16}$$

One thing we have to pay attention at this point is the sign of the interferometer reflectivity for the rf sideband $r_{\rm sb}$ because it drastically changes the frequency shape produced by the zero-pole pair. As for the 9 MHz rf sideband, $r_{\rm sb}$ is a positive number somewhat close to unity which indicates that the interferometer is highly over-coupled. On the other hand, since the 45 MHz is slightly under-coupled, $r_{\rm sb}$ is a negative number while large fraction of the field is transmitted to the AS port by design. Therefore according to the last equation, $\omega_{\rm r}$ can be negative for the 9 MHz. In fact, the phase plot in figure 4 show that $\omega_{\rm r}$ is a negative zero for the signals demodulated at 9 MHz. As opposed to the 9 MHz demodulated signals, the one for the 45 MHz has a positive zero which is higher than $\omega_{\rm cc}$ as shown in the plot.

The SRCL signal is a flat response because it does not contains the carrier audio sidebands. In fact, it is not able to excite the carrier audio sidebands at all in this particular case because there is no carrier light in the signal recycling cavity. The sign of the response changes between the 9 and 45 MHz rf sidebands. This is due to the fact that they have opposite interference conditions in the signal recycling cavity.

4.3 POP port

The signals at the POP port are similar to that of REFL. In fact, all the DOFs maintain the same frequency shape to that of REFL except for the PRCL response. The response can be summarized as,

$$\begin{aligned}\frac{S^{(\rm pop)}}{S_0} =& \frac{4g_{\rm p}^2 g_{\rm sb} r'_{\rm a} r_{\rm sm}}{t_{\rm p}} \frac{1}{1+i\omega/\omega_{\rm cc}} k\Delta L_+ \cos\omega_{\rm m} t \\ &+ 4\frac{g_{\rm p} g_{\rm sb}^2 r_{\rm a} \hat{r_{\rm a}}'}{t_{\rm p}} \chi k\Delta L_- \sin\omega_{\rm m} t \\ &- 4\frac{g_{\rm p} g_{\rm sb}^2 r_{\rm a} \hat{r_{\rm a}}}{t_{\rm p}} \chi k\Delta l_- \sin\omega_{\rm m} t \\ &+ 4\left(g_{\rm p} - g_{\rm sb}\right) \frac{g_{\rm p} g_{\rm sb} r_{\rm a} r_{\rm sm}}{t_{\rm p}} \frac{1+i\omega/\omega_{\rm p}}{1+i\omega/\omega_{\rm cc}} k\Delta l_{\rm p} \cos\omega_{\rm m} t \\ &\pm 4\frac{g_{\rm p} g_{\rm sb}^2 r_{\rm a} r_{\rm s} t_{\rm sm}^2}{t_{\rm p} t_{\rm s}^2} k\Delta l_{\rm s} \cos\omega_{\rm m} t,\end{aligned} \tag{17}$$

where the zero in the PRCL response is defined as

$$\omega_{\rm p} = \omega_{\rm cc}\left(1 - \frac{g_{\rm p}}{g_{\rm sb}}\right). \tag{18}$$

We have the same trick as iLIGO for the PRCL readout – a very large suppression of CARM using REFL9 reshapes the response of PRCL in POP [1]. Ignoring the differential and SRCL signals and making the left hand side of equation (13) to zero, one can find a relation between ΔL_+ and $\Delta l_{\rm p}$. Plugging the relation into the POP response (17), one can rewrite the PRCL signal as

$$\left.\frac{S^{(\rm pop)}}{S_0}\right|_{\rm refl\to 0} = 4\frac{g_{\rm sb}^2 r_{\rm sm}}{r_{\rm sb}t_{\rm p}}\left(g_{\rm p}r_{\rm a}r_{\rm sb} + g_{\rm sb}r_{\rm c}r_{\rm sm}\right)k\Delta l_{\rm p}\cos\omega_{\rm m}t. \tag{19}$$

As was the case in iLIGO, the POP signal becomes frequency independent in the presence of the high gain CARM loop.

4.4 Laser frequency and intensity noises

As long as both DARM and CARM are locked on the operating point with perfectly matched two arm cavities, neither frequency or intensify noise of the laser couple to the signals in the AS signal. We plant to discuss noise couplings of laser noises in the next part of the study.

Apart from the AS port, the laser frequency can be detected at the REFL and POP ports as follows,

$$\begin{aligned}\frac{S^{(\rm refl)}}{S_0} &= -\frac{8\pi L g_{\rm p}^2 r'_{\rm a} r_{\rm sb}}{c}\frac{1}{1+i\omega/\omega_{\rm cc}}\Delta\nu\cos\omega_{\rm m}t,\\ \frac{S^{(\rm pop)}}{S_0} &= \frac{8\pi L g_{\rm p}^2 g_{\rm sb} r_{\rm sm} r'_{\rm a}}{ct_{\rm p}}\frac{1}{1+i\omega/\omega_{\rm cc}}\Delta\nu\cos\omega_{\rm m}t.\end{aligned} \tag{20}$$

Comparing these results with equations (13) and (17), one can easily confirm that a small deviation in the common mode of the arms ΔL_+ is related to a small change in the laser frequency $\Delta\nu$ through the famous conversion relation,

$$\frac{\Delta\nu}{\nu_0} = \frac{\Delta L_+}{L}, \tag{21}$$

where ν_0 is the laser frequency defined as $\nu_0 = kc/2\pi$.

5 Comparison with iLIGO

Since the responses we derived in the previous section are written in analytic form, we can perform an interesting verification test – we scale down the responses to that of iLIGO. In order to to do it, one simply needs to remove the signal recycling mirror out of the equations by setting $r_{\rm s} \to 0$ and $t_{\rm s} \to 1$. According to equations (4), (6), (12) and (14), one can simplify the following quantities as,

$$\begin{aligned} \omega_{\rm rse} &\to \omega_{\rm c}, \quad g_{\rm s} \to 1, \\ \chi \to \sin\left(\frac{2\omega l_{\rm sch}}{c}\right), \quad r_{\rm sm} &\to r_{\rm M}, \quad t_{\rm sm} \to t_{\rm M}, \end{aligned} \tag{22}$$

where $\omega_{\rm c}$ is the cavity pole for a single arm, defined as

$$\omega_{\rm c} = \frac{c}{2L} \ln\left(\frac{1}{r_{\rm i} r_{\rm e}}\right). \tag{23}$$

Since we now removed the signal recycling mirror, there essentially is no difference between the 9 and 45 MHz rf sidebands. Therefore we consider only one rf frequency.

Plugging the above quantities back into equation (11), the response at AS can be now rewritten as,

$$\begin{aligned} \left.\frac{S^{(\rm as)}}{S_0}\right|_{\rm iLIGO} \to &- 4 g_{\rm p} g_{\rm sb} r'_{\rm a} t_{\rm M} \frac{1}{1 + i\omega/\omega_{\rm c}} k \Delta L_- \sin\omega_{\rm m} t \\ &- 4 g_{\rm p} g_{\rm sb} r_{\rm a} t_{\rm M} \frac{1}{1 + i\omega/\omega_{\rm c}} k \Delta l_- \sin\omega_{\rm m} t. \end{aligned} \tag{24}$$

This is the same as what reference [1] shows, except for two points – they assumed $\hat{r_{\rm a}} = -1$ and used a different sign convention for arms' reflectivity $r_{\rm a}$ and Michelson transmissivity $t_{\rm M}$.

In the same way, one can reduce the REFL and POP signals to equivalent of iLIGO as well,

$$\begin{aligned}\left.\frac{S^{(\mathrm{refl})}}{S_0}\right|_{\mathrm{iLIGO}} \rightarrow & -4g_{\mathrm{p}}^2 r_{\mathrm{a}}' r_{\mathrm{sb}} \frac{1}{1+i\omega/\omega_{\mathrm{cc}}} k\Delta L_+ \cos\omega_{\mathrm{m}} t \\ & + 4g_{\mathrm{sb}}^2 r_{\mathrm{c}} \hat{r_{\mathrm{a}}}' \sin\left(\frac{2\omega_{\mathrm{m}} l_{\mathrm{sch}}}{c}\right) k\Delta L_- \sin\omega_{\mathrm{m}} t \\ & - 4g_{\mathrm{sb}}^2 r_{\mathrm{c}} \hat{r_{\mathrm{a}}} \sin\left(\frac{2\omega_{\mathrm{m}} l_{\mathrm{sch}}}{c}\right) k\Delta l_- \sin\omega_{\mathrm{m}} t \\ & - 4\left(g_{\mathrm{p}}^2 r_{\mathrm{a}} r_{\mathrm{sb}} + g_{\mathrm{sb}}^2 r_{\mathrm{c}} r_{\mathrm{M}}\right) \frac{1+i\omega/\omega_{\mathrm{r}}}{1+i\omega/\omega_{\mathrm{cc}}} k\Delta l_{\mathrm{p}} \cos\omega_{\mathrm{m}} t.\end{aligned} \tag{25}$$

$$\begin{aligned}\left.\frac{S^{(\mathrm{pop})}}{S_0}\right|_{\mathrm{iLIGO}} \rightarrow & \frac{4g_{\mathrm{p}}^2 g_{\mathrm{sb}} r_{\mathrm{a}}' r_{\mathrm{M}}}{t_{\mathrm{p}}} \frac{1}{1+i\omega/\omega_{\mathrm{cc}}} k\Delta L_+ \cos\omega_{\mathrm{m}} t \\ & + 4\frac{r_{\mathrm{a}} \hat{r_{\mathrm{a}}}' g_{\mathrm{p}} g_{\mathrm{sb}}^2}{t_{\mathrm{p}}} \sin\left(\frac{2\omega_{\mathrm{m}} l_{\mathrm{sch}}}{c}\right) k\Delta L_- \sin\omega_{\mathrm{m}} t \\ & - 4\frac{r_{\mathrm{a}} \hat{r_{\mathrm{a}}} g_{\mathrm{p}} g_{\mathrm{sb}}^2}{t_{\mathrm{p}}} \sin\left(\frac{2\omega_{\mathrm{m}} l_{\mathrm{sch}}}{c}\right) k\Delta l_- \sin\omega_{\mathrm{m}} t \\ & + 4\left(g_{\mathrm{p}} - g_{\mathrm{sb}}\right) \frac{g_{\mathrm{p}} g_{\mathrm{sb}} r_{\mathrm{a}} r_{\mathrm{M}}}{t_{\mathrm{p}}} \frac{1+i\omega/\omega_{\mathrm{p}}}{1+i\omega/\omega_{\mathrm{cc}}} k\Delta l_{\mathrm{p}} \cos\omega_{\mathrm{m}} t.\end{aligned} \tag{26}$$

They are the same as what the previous study says.

6 Conclusions and prospects

We derived a set of analytic equations that describe the frequency responses of the aLIGO interferometer to all five interferometric degrees of freedom. Similarly to iLIGO, the PRCL response in POP is reshaped by the CARM loop suppressing the REFL signal with a very high gain. This results in a flat response for PRCL as was the case in iLIGO. The responses can be scaled to a no-SRM case in which we can indirectly check validation of the analytic expressions by comparing them with those from the previous study for iLIGO. We confirmed that the expressions can be scaled back to that of iLIGO without a conflict.

In the next document, namely part II, we will include a DARM offset in order to make the configuration more realistic. This will consequently introduce at least one major change to the responses. It is going to dramatically change the SRCL response in the REFL and POP

ports because the DARM offset will allow SRCL for exciting the carrier light. In addition, we will investigate the noise coupling of laser noises to the AS port with some realistic asymmetries.

CARM

	$dE^{(c)} \otimes E^{(sb)}$	$E^{(c)} \otimes dE^{(sb)}$	**leading term**
REFL 9I	∃	∃	$dE^{(c)} \otimes E^{(sb)}$
REFL 9Q	-	-	-
REFL 45I	∃	∃	$dE^{(c)} \otimes E^{(sb)}$
REFL 45Q	-	-	-
POP 9I	∃	∃	$dE^{(c)} \otimes E^{(sb)}$
POP 9Q	-	-	-
POP 45I	∃	∃	$dE^{(c)} \otimes E^{(sb)}$
POP 45Q	-	-	-
AS 9I	-	-	-
AS 9Q	-	-	-
AS 45I	-	-	-
AS 45Q	-	-	-

DARM

	$dE^{(c)} \otimes E^{(sb)}$	$E^{(c)} \otimes dE^{(sb)}$	**leading term**
REFL 9I	-	-	-
REFL 9Q	-	∃	$E^{(c)} \otimes dE^{(sb)}$
REFL 45I	-	-	-
REFL 45Q	-	∃	$E^{(c)} \otimes dE^{(sb)}$
POP 9I	-	-	-
POP 9Q	-	∃	$E^{(c)} \otimes dE^{(sb)}$
POP 45I	-	-	-
POP 45Q	-	∃	$E^{(c)} \otimes dE^{(sb)}$
AS 9I	-	-	-
AS 9Q	∃	-	$dE^{(c)} \otimes E^{(sb)}$
AS 45I	-	-	-
AS 45Q	∃	-	$dE^{(c)} \otimes E^{(sb)}$

MICH

	$dE^{(c)} \otimes E^{(sb)}$	$E^{(c)} \otimes dE^{(sb)}$	**leading term**
REFL 9I	-	-	-
REFL 9Q	-	∃	$E^{(c)} \otimes dE^{(sb)}$
REFL 45I	-	-	-
REFL 45Q	-	∃	$E^{(c)} \otimes dE^{(sb)}$
POP 9I	-	-	-
POP 9Q	-	∃	$E^{(c)} \otimes dE^{(sb)}$
POP 45I	-	-	-
POP 45Q	-	∃	$E^{(c)} \otimes dE^{(sb)}$
AS 9I	-	-	-
AS 9Q	∃	-	$dE^{(c)} \otimes E^{(sb)}$
AS 45I	-	-	-
AS 45Q	∃	-	$dE^{(c)} \otimes E^{(sb)}$

PRCL

	$dE^{(c)} \otimes E^{(sb)}$	$E^{(c)} \otimes dE^{(sb)}$	**leading term**
REFL 9I	∃	∃	both
REFL 9Q	-	-	-
REFL 45I	∃	∃	both
REFL 45Q	-	-	-
POP 9I	∃	∃	both
POP 9Q	-	-	-
POP 45I	∃	∃	both
POP 45Q	-	-	-
AS 9I	-	-	-
AS 9Q	-	-	-
AS 45I	-	-	-
AS 45Q	-	-	-

SRCL

REFL 9I	-	∃	$E^{(c)} \otimes dE^{(sb)}$
REFL 9Q	-	-	-
REFL 45I	-	∃	$E^{(c)} \otimes dE^{(sb)}$
REFL 45Q	-	-	-
POP 9I	-	∃	$E^{(c)} \otimes dE^{(sb)}$
POP 9Q	-	-	-
POP 45I	-	∃	$E^{(c)} \otimes dE^{(sb)}$
POP 45Q	-	-	-
AS 9I	-	-	-
AS 9Q	-	-	-
AS 45I	-	-	-
AS 45Q	-	-	-

Table 2: Summary of all the responses. The elements filled with ∃ means that they have non-zero values, otherwise zero signals.

A Response at DC

As stated in equation (8), the demodulated signals are made of $dE^{(c)} \otimes E^{(sb)}$ and $E^{(c)} \otimes dE^{(sb)}$. In section 4, we have dealt $dE^{(c)}$ and $dE^{(sb)}$ as audio sidebands which were excited by a length modulation at frequency ω. Here, instead, we consider these small deviations as slow motion or an audio sideband at DC. This method reduces the complexity of the algebra somewhat and therefore can provide a relatively quick verification for the frequency responses.

We divide the calculation process of the method into three steps according to how we derive the responses as written in equation (8). As a first step, in section A.1, we compute the static fields i.e. $E^{(c)}$ and $E^{(sb)}$ at the detection ports. As a next step in section A.2, we derive the static response of the fields with respect to a change in each length DOF. This gives us $dE^{(c)}$ and $dE^{(sb)}$. Finally, in section A.3, we combine the results of the previous two sections to produce the responses.

A.1 Static fields at the detection port

The reflectivity of the whole interferometer and the signal-recycled Michelson for rf sidebands (i.e. r_{sb} and r_{sm}) do not change the sign regardless of whether it is for a upper or lower rf sideband. So for the reason, the following equations can be applied to both upper and lower sidebands.

$$\begin{aligned} E^{(c)}_{REFL} &= J_0 r_c E_0, \\ E^{(sb)}_{REFL} &= i J_1 r_{sb} E_0. \end{aligned} \tag{27}$$

$$\begin{aligned} E^{(c)}_{POP} &= J_0 g_p r_a E_0, \\ E^{(sb)}_{POP} &= -i J_1 g_{sb} r_{sm} E_0. \end{aligned} \tag{28}$$

On the other hand, the sign of the transmissivity of the signal-recycled Michelson t_{sm} is sensitive to whether it is upper or lower rf sideband because it is proportional to term

$\sin(l_{\rm sch}\omega_{\rm m}/c)$. So for the reason, the static rf fields at the AS port need a special care as,

$$\begin{aligned} E_{\rm AS}^{\rm (c)} &= 0, \\ E_{\rm AS}^{\rm (sb)} &= \begin{cases} J_1 g_{\rm sb} t_{\rm sm} E_0 & \text{(for upper rf sideband)} \\ -J_1 g_{\rm sb} t_{\rm sm} E_0 & \text{(for lower rf sideband)} \end{cases}, \end{aligned} \tag{29}$$

where we have taken out the phase delay due to the propagation of the light to the AS port.

A.2 Response of the fields to small displacements

When the length DOFs are statically displaced, the carrier field at the detection ports deviate from their nominal values by the following amount,

$$\begin{pmatrix} \Delta E_{\rm AS}^{\rm (c)} \\ \Delta E_{\rm REFL}^{\rm (c)} \\ \Delta E_{\rm POP}^{\rm (c)} \end{pmatrix} = 2kJ_0 \begin{bmatrix} 0 & ig_{\rm p}g_{\rm s}r'_{\rm a} & ig_{\rm p}g_{\rm s}r_{\rm a} & 0 & 0 \\ -ig_{\rm p}^2 r'_{\rm a} & 0 & 0 & -ig_{\rm p}^2 r_{\rm a} & 0 \\ -ig_{\rm p}^2 r_{\rm a}/t_{\rm p} & 0 & 0 & -ig_{\rm p}^2 r_{\rm a}/t_{\rm p} & 0 \end{bmatrix} \begin{pmatrix} \Delta L_+ \\ \Delta L_- \\ \Delta l_- \\ \Delta l_{\rm p} \\ \Delta l_{\rm s} \end{pmatrix}. \tag{30}$$

As for the rf sidebands, deviations can be found as,

$$\Delta E_{\rm AS}^{\rm (sb)} = 2J_1 k E_0 \begin{pmatrix} -ig_{\rm sb}^2 \hat{r_{\rm a}}' t_{\rm s}\rho_{\rm c}/t_{\rm p} \\ -g_{\rm sb}^2 \hat{r_{\rm a}}' \rho_{\rm d} t_{\rm s}/t_{\rm p} \\ +g_{\rm sb}^2 \hat{r_{\rm a}} \rho_{\rm d} t_{\rm s}/t_{\rm p} \\ -ig_{\rm sb}^2 r_{\rm p} r_{\rm sm} t_{\rm sm}/t_{\rm p} \\ -ig_{\rm sb}^2 r_{\rm s} t_{\rm sm}^2 \rho_{\rm s}/t_{\rm p} \end{pmatrix}^{\mathsf{T}} \cdot \begin{pmatrix} \Delta L_+ \\ \Delta L_- \\ \Delta l_- \\ \Delta l_{\rm p} \\ \Delta l_{\rm s} \end{pmatrix} \tag{31}$$

$$\Delta E^{(\mathrm{sb})}_{\mathrm{REFL}} = 2J_1 k E_0 \begin{pmatrix} \Theta g^2_{\mathrm{sb}} \hat{r_{\mathrm{a}}}' \\ -i\chi g^2_{\mathrm{sb}} \hat{r_{\mathrm{a}}}' \\ i\chi g^2_{\mathrm{sb}} \hat{r_{\mathrm{a}}} \\ -g^2_{\mathrm{sb}} r_{\mathrm{sm}} \\ g^2_{\mathrm{sb}} r_{\mathrm{s}} t^2_{\mathrm{sm}} / t^2_{\mathrm{s}} \end{pmatrix}^{\mathsf{T}} \cdot \begin{pmatrix} \Delta L_+ \\ \Delta L_- \\ \Delta l_- \\ \Delta l_{\mathrm{p}} \\ \Delta l_{\mathrm{s}} \end{pmatrix} \tag{32}$$

$$\Delta E^{(\mathrm{sb})}_{\mathrm{POP}} = \frac{2J_1 k E_0}{t_p} \begin{pmatrix} \Theta g^2_{\mathrm{sb}} \hat{r_{\mathrm{a}}}' \\ -i\chi g^2_{\mathrm{sb}} \hat{r_{\mathrm{a}}}' \\ i\chi g^2_{\mathrm{sb}} \hat{r_{\mathrm{a}}} \\ -g^2_{\mathrm{sb}} r_{\mathrm{sm}} \\ g^2_{\mathrm{sb}} r_{\mathrm{s}} t^2_{\mathrm{sm}} / t^2_{\mathrm{s}} \end{pmatrix}^{\mathsf{T}} \cdot \begin{pmatrix} \Delta L_+ \\ \Delta L_- \\ \Delta l_- \\ \Delta l_{\mathrm{p}} \\ \Delta l_{\mathrm{s}} \end{pmatrix} \tag{33}$$

where,

$$\begin{aligned} \rho_{\mathrm{c}} &\equiv \frac{1 \mp r_{\mathrm{s}} \hat{r_{\mathrm{a}}}}{\left(1 \mp r_{\mathrm{s}} \hat{r_{\mathrm{a}}} \cos\phi_{\mathrm{sch}}\right)^2} \sin\phi_{\mathrm{sch}}, \\ \rho_{\mathrm{d}} &\equiv \frac{-\cos\phi_{\mathrm{sch}} - \hat{r_{\mathrm{a}}}\left(r_{\mathrm{p}} \mp r_{\mathrm{s}}\right) \pm r_{\mathrm{p}} r_{\mathrm{s}} \hat{r_{\mathrm{a}}}^2}{\left(1 \mp r_{\mathrm{s}} \hat{r_{\mathrm{a}}} \cos\phi_{\mathrm{sch}}\right)^2}, \\ \rho_{\mathrm{s}} &\equiv \frac{-r_{\mathrm{p}} \hat{r_{\mathrm{a}}} - \cos\phi_{\mathrm{sch}}}{t_{\mathrm{s}} \sin\phi_{\mathrm{sch}}}, \\ \Theta &\equiv \frac{\left(1 + r_{\mathrm{s}}^2 \hat{r_{\mathrm{a}}}^2\right)\cos\phi_{\mathrm{sch}} \mp 2 r_{\mathrm{s}} \hat{r_{\mathrm{a}}}}{\left(1 \mp r_{\mathrm{s}} \hat{r_{\mathrm{a}}} \cos\phi_{\mathrm{sch}}\right)^2}. \end{aligned} \tag{34}$$

A.3 Static Responses

The static responses can be derived by the following exression,

$$S = 2\mathrm{Re}\left[\left(E^{(\mathrm{lsb})*}\Delta E^{(\mathrm{c})} + \Delta E^{(\mathrm{c})*} E^{(\mathrm{usb})} + \Delta E^{(\mathrm{lsb})*} E^{(\mathrm{c})} + E^{(\mathrm{c})*}\Delta E^{(\mathrm{usb})}\right) e^{i\omega_m t}\right] \tag{35}$$

Substituting the results from the previous two subsections to the above equation, one can

obtain the responses as follows,

$$\begin{aligned}\frac{S^{(\mathrm{as})}}{S_0} =& -4g_{\mathrm{p}}g_{\mathrm{s}}g_{\mathrm{sb}}r'_{\mathrm{a}}t_{\mathrm{sm}}k\Delta L_- \sin\omega_{\mathrm{m}}t \\ & -4g_{\mathrm{p}}g_{\mathrm{s}}g_{\mathrm{sb}}r_{\mathrm{a}}t_{\mathrm{sm}}k\Delta l_- \sin\omega_{\mathrm{m}}t\end{aligned} \tag{36}$$

$$\begin{aligned}\frac{S^{(\mathrm{refl})}}{S_0} =& -4\left(g_{\mathrm{p}}^2 r'_{\mathrm{a}}r_{\mathrm{sb}} - g_{\mathrm{sb}}^2 \hat{r_{\mathrm{a}}}' r_{\mathrm{c}}\Theta\right) k\Delta L_+ \cos\omega_{\mathrm{m}}t \\ & +4\chi g_{\mathrm{sb}}^2 r_{\mathrm{c}}\hat{r_{\mathrm{a}}}' k\Delta L_- \sin\omega_{\mathrm{m}}t \\ & -4\chi g_{\mathrm{sb}}^2 r_{\mathrm{c}}\hat{r_{\mathrm{a}}} k\Delta l_- \sin\omega_{\mathrm{m}}t \\ & -4\left(g_{\mathrm{p}}^2 r_{\mathrm{a}}r_{\mathrm{sb}} + g_{\mathrm{sb}}^2 r_{\mathrm{c}}r_{\mathrm{sm}}\right) k\Delta l_{\mathrm{p}} \cos\omega_{\mathrm{m}}t \\ & \pm 4\frac{g_{\mathrm{sb}}^2 r_{\mathrm{c}}r_{\mathrm{s}}t_{\mathrm{sm}}^2}{t_{\mathrm{s}}^2} k\Delta l_{\mathrm{s}} \cos\omega_{\mathrm{m}}t\end{aligned} \tag{37}$$

$$\begin{aligned}\frac{S^{(\mathrm{pop})}}{S_0} =& \frac{4g_{\mathrm{p}}g_{\mathrm{sb}}}{t_{\mathrm{p}}}\left(g_{\mathrm{p}}r'_{\mathrm{a}}r_{\mathrm{sm}} + g_{\mathrm{sb}}\hat{r_{\mathrm{a}}}' r_{\mathrm{a}}\Theta\right) k\Delta L_+ \cos\omega_{\mathrm{m}}t \\ & +4\frac{\chi g_{\mathrm{p}}g_{\mathrm{sb}}^2 r_{\mathrm{a}}\hat{r_{\mathrm{a}}}'}{t_{\mathrm{p}}} k\Delta L_- \sin\omega_{\mathrm{m}}t \\ & -4\frac{\chi g_{\mathrm{p}}g_{\mathrm{sb}}^2 r_{\mathrm{a}}\hat{r_{\mathrm{a}}}}{t_{\mathrm{p}}} k\Delta l_- \sin\omega_{\mathrm{m}}t \\ & +4\frac{g_{\mathrm{p}}g_{\mathrm{sb}}r_{\mathrm{a}}r_{\mathrm{sm}}}{t_{\mathrm{p}}}\left(g_{\mathrm{p}} - g_{\mathrm{sb}}\right) k\Delta l_{\mathrm{s}} \cos\omega_{\mathrm{m}}t \\ & \pm 4\frac{g_{\mathrm{sb}}^2 g_{\mathrm{p}}r_{\mathrm{a}}r_{\mathrm{s}}t_{\mathrm{sm}}^2}{t_{\mathrm{p}}t_{\mathrm{s}}^2} k\Delta l_{\mathrm{s}} \cos\omega_{\mathrm{m}}t\end{aligned} \tag{38}$$

As shown in the above equations, the coefficient of the CARM responses in the REFL and POP ports are different from what we had in the full frequency-dependent expressions (13) and (17). This is because we dropped off the $E^{(\mathrm{c})} \otimes dE^{(\mathrm{sb})}$ term in the full frequency-dependent expressions as they are negligible compared with $dE^{(\mathrm{c})} \otimes E^{(\mathrm{sb})}$.

B Numerical parameters

symbol	description	value
$T_{\rm i}$	ITM power transmissivity	0.0141
$\lambda_{\rm i}$	ITM loss on the HR surface	0
$t_{\rm i}$	ITM amplitude transmissivity or $\sqrt{T_{\rm i}}$	
$r_{\rm i}$	ITM amplitude reflectivity or $\sqrt{1-T_{\rm i}-\lambda_{\rm i}}$	
$T_{\rm e}$	ETM power trasmissivity	50e-6
$\lambda_{\rm e}$	ETM loss on the HR surface	0
$t_{\rm e}$	ETM amplitude transmissivity or $\sqrt{T_{\rm e}}$	
$r_{\rm e}$	ETM amplitude reflectivity or $\sqrt{1-T_{\rm e}-\lambda_{\rm e}}$	
$T_{\rm p}$	PRM power trasmissivity	0.031
$\lambda_{\rm p}$	PRM loss on the HR surface	0
$t_{\rm p}$	PRM amplitude transmissivity or $\sqrt{T_{\rm p}}$	
$r_{\rm p}$	PRM amplitude reflectivity or $\sqrt{1-T_{\rm p}-\lambda_{\rm p}}$	
$T_{\rm s}$	SRM power trasmissivity	0.37
$\lambda_{\rm s}$	SRM loss on the HR surface	0
$t_{\rm s}$	SRM amplitude transmissivity or $\sqrt{T_{\rm s}}$	
$r_{\rm s}$	SRM amplitude reflectivity or $\sqrt{1-T_{\rm s}-\lambda_{\rm s}}$	
	optical distances	
$L_{\rm arm}$	arm length (both X and Y)	3994.5 m
$l_{\rm sch}$	Schnupp asymmetry $(l_x - l_y)/2$	0.04 m
$l_{\rm p}$	Power recycling cavity length	57.65 m
$l_{\rm s}$	Signal recycling cavity length	56.0 m
	Laser property	
$P_{\rm in}$	input laser power	1 W
f_1	modulation frequency of the first rf sideband	9099451 Hz
f_2	modulation frequency of the second rf sideband	45497255 Hz
Γ_1	modulation depth of the f_1 rf sideband	0.1 rad
Γ_2	modulation depth of the f_2 rf sideband	0.1 rad

Table 3: Summary of the numerical paramters.

References

[1] Daniel Sigg, "Frequency Response of the LIGO Interferometer", LIGO-T970084 (1997)

[2] Peter Fritschel et al., "Readout and control of a power-recycled interferometric gravitational-wave antenna", Applied Optics, 40 28 (2001)

[3] The LIGO Scientific Collaboration, "Advanced LIGO", Class. Quantum Grav., 32 074001 (2015)

[4] Eric D. Black and Ryan N. Gutenkunst, "An Introduction to Signal Extraction in Interferometric Gravitational-Wave Detectors", LIGO-P020029 (2002)

[5] Martin Regehr, "Signal Extraction and Control for an Interferometric Gravitational Wave Detector", Thesis, Caltech (1995)